RSC Advances

PAPER

View Article Online
View Journal | View Issue

Cite this: *RSC Adv.*, 2015, **5**, 31972

Novel multi-sensitive pseudo-poly(amino acid) for effective intracellular drug delivery†

Yanjuan Wu,[ab] Dongfang Zhou,[a] Yanxin Qi,[a] Zhigang Xie,[a] Xuesi Chen,[a] Xiabin Jing[a] and Yubin Huang*[a]

Received 25th February 2015
Accepted 27th March 2015

DOI: 10.1039/c5ra03423j

www.rsc.org/advances

Novel intracellular pH, glutathione (GSH) and reactive oxygen species (ROS)-responsive nanoparticles were obtained using mPEG$_{2k}$-*block*-redox dual sensitive chain-*block*-mPEG$_{2k}$ (PRDSP) which was prepared by Cu(I)-catalyzed azide–alkyne cycloaddition (CuAAC) click polymerization. The disulfide bond, peroxalate ester and triazole units were regularly and repeatedly arranged in the hydrophobic blocks. The disulfide bond was GSH-sensitive and the peroxalate ester structure could be disrupted by acid and hydrogen peroxide. In addition, the triazole units are capable of forming pH-responsive hydrogen bonds. Dynamic Light Scattering (DLS) and transmission electron microscopy (TEM) were used to investigate the pH, GSH and ROS sensitivity of the PRDSP nanoparticles (NPs). The results indicated that the average diameter, size distribution and morphology greatly changed upon adding GSH/H_2O_2 or modulating the pH. As the preloaded model anticancer drug, doxorubicin (DOX) was quickly released from DOX-loaded PRDSP (PRDSP@DOX) NPs by addition of 10 mM glutathione (GSH), or 10 mM H_2O_2 or under acidic conditions rather than under physiological conditions. Confocal laser scanning microscopy (CLSM) and flow cytometric analyses revealed that PRDSP@DOX could effectively deliver DOX into the cytoplasm and nucleus of cells. Therefore, PRDSP NPs may be a promising redox heterogeneity-sensitive carrier for efficient and controlled anticancer drug release.

Introduction

Nano-scaled functional polymeric nanocarriers offer several unique features, such as improving drug bioavailability and solubility, decreasing side effects, and preferential accumulation at tumor sites *via* the enhanced permeability and retention (EPR) effect. Therefore, in the past decades, functional polymeric materials have emerged as a most viable and promising controlled drug delivery system (DDS) for cancer treatment.

Multifarious stimuli-responsive DDSs have been extensively studied.[1–7] Of these DDSs, the block copolymer micelle is one of the most important species because of their palpable advantages, including viable modularization, ordinary synthetic procedures and characterizations, and simple self-assemble process. Consequently, enormous efforts have been made to the development of block copolymer micelles in response to internal stimulus (*e.g.* pH, reductive potential, glucose, oxidative stress, and lysosomal enzymes) or external stimulus (*e.g.* light, magnetic field, and ultrasound).[8–12] For example, pH levels in late endosomes (pH 5.0–6.0) and lysosomes (pH ~ 5.0) are notably lower than normal extracellular pH (~7.4). Taking advantages of slightly acidic environments, enormous pH-sensitive block copolymers have been developed to realize enhanced drug release at tumor site.[13,14] In addition, cancer cells may have the millimolar level of intracellular glutathione (GSH), which is reported to be several-fold higher than that of plasma GSH. Zhong's groups had introduced disulfide bonds into the main chain, cross-linking unit or side chain of the block copolymer micelles for rapid intracellular release of anticancer drugs.[15–17] It should be further noted that low or intermediate levels of ROS are endogenous class of carcinogens, causing DNA damage, cell mutation and promoting cell proliferation, and ultimately inducing carcinogenesis.[18] The high oxidative stress in the cytosol and cell nuclei of tumor cells have recently been exploited for active intracellular release of various drugs.[19–22]

Despite the considerable development of various stimuli-sensitive block copolymers, few of the DDSs have achieved optimal outcomes. The challenges still exist. First, an ideal controllable DDS should be fast but not burst release. In most reported copolymer systems, stimuli-sensitive bonds located either in the cross-linking unit, or on the side chain, or in the main chain with limited number (like only one such bond in the main chain).[23,24] Therefore, under the environmental stimuli, the assembly structure of the drug-loading system could not be

[a]*State Key Laboratory of Polymer Physics and Chemistry, Changchun Institute of Applied Chemistry, Chinese Academy of Sciences, Changchun 130022, P. R. China. E-mail: ybhuang@ciac.jl.cn; Fax: +86 431 85262769; Tel: +86 431 85262769*

[b]*Graduate University of the Chinese Academy of Sciences, Beijing 100039, P. R. China*

† Electronic supplementary information (ESI) available: ^{1}H NMR spectra, FT-TR spectra, GPC spectra, a representative CAC plot of PRDSP, DLS and TEM images, other *in vitro* cellular data. See DOI: 10.1039/c5ra03423j

entirely destroyed, leading to a slow but incomplete drug release. Drug efficiency is another crucial point. High drug loading content (DLC) and drug loading efficiency (DLE) are commonly necessary. However, most stimuli-responsive bonds could not provide additional interaction with the loaded drugs to improve DLC and DLE levels. The most important challenge is the heterogeneity of cancer cells.[25] For example, different stimuli may coexist in one cancer cell, but also may exist in different regions of tumor site. Furthermore, one cancer cell may has different stimuli levels at different living stages. Thus, nanocarriers bearing single sensitivity may not sufficiently release the loaded drugs under the complex situation of internal stimuli inside tumor cells, leading to unsatisfied therapeutic efficacy. For these reasons, design of multi-responsive block copolymers becomes rational and available.

In this work, a novel redox dual sensitive polymer was designed and synthesized by introducing disulfide bonds and peroxalate ester units repeatedly into polymer backbone. To our best knowledge, conventional polymerization methods, such as ring opening polymerization (ROP), could also be used to synthesize multi-responsive nanocarrier. However, the stimuli-sensitive bonds were usually arranged in the copolymer randomly. We noticed that Cu(I)-catalyzed azide–alkyne cycloaddition (CuAAC) click polymerization was generally used to synthesize functional polymer due to its ordinary manipulation, gentle reaction condition, selectivity and orthogonality with various functional groups.[26–30] CuAAC click polymerization is a very convenient tool to import two or more functions into one system. Plenty of triazole groups formed in polymer backbone could be served as hydrogen bond acceptors and donors. In our design, cystine, a natural amino acid with one disulfide group, was chosen as starting material to synthesis dialkyned monomer first. Then peroxalate ester unit was imported into the diazided monomer. After CuAAC click polymerization under the catalysis of CuCl/PMDETA, the prepared hydrophobic block was further reacted with azide-terminated $mPEG_{2k}$ to obtain an ABA-type triblock copolymer (PRDSP). In this PRDSP copolymer, disulfide, peroxalate ester and triazole units were repeatedly interposed into polymer backbone without any protection and deprotection steps. Because of the sensitive characteristics, this polymer could be degraded by enzyme and disrupted under redox circumstance. The existence of triazole groups may form hydrogen bond and also involve the electrostatic interaction with DOX to improve the drug loading efficiency. DOX was loaded into

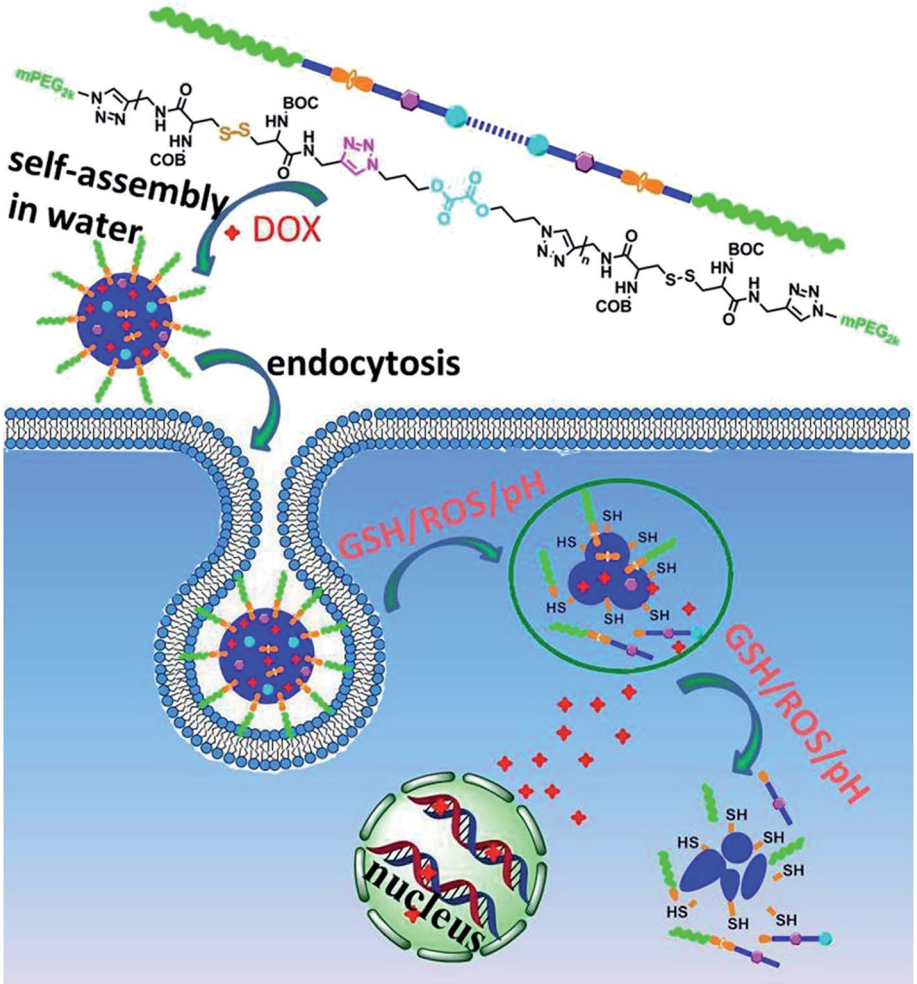

Scheme 1 Schematic illustration of DOX loading, endocytosis and intracellular microenvironment triggered release from PRDSP@DOX NPs.

PRDSP NPs as a model drug. The DOX loading, endocytosis and intracellular drug release were presented in Scheme 1. The effective loading of DOX and triggered release in response to different pH values, distinct concentrations of GSH and disparate H_2O_2 level were demonstrated. The intracellular pH, GSH, ROS multi-sensitive pseudo-poly(amino acid) NPs may be potential candidates as platforms for intracellular drug delivery.

Experimental section

Materials

Cuprous chloride (CuCl) was purified following the prior experimental manipulation. *N*,*N*-Di(*tert*-butoxycarbonyl)-L-cystine (BOC-cystine) was synthesized according to traditional procedure. Poly(ethylene glycol) methyl ether with an M_n of *ca.* 2000, 3-chloro-1-propanol, mesyl chloride and proparygl amine were purchased from Sigma-Aldrich and used without further purification. L-Cystine and (benzotriazol-1-yloxy)tris(dimethylamino) phosphoniumhexafluophosphate (BOP reagent) were obtained from GL Biochem (Shanghai) Ltd. *N*,*N*,*N*′,*N*″,*N*″-Pentamethyldiethylenetriamine (PMDETA), 4-dimethylaminopyridine and oxalyl chloride were purchased from Aladdin (Shanghai) Ltd. Sodium azide (NaN_3) and glutathione (GSH) were obtained from Energy Chemical (Shanghai) Ltd. Doxorubicin hydrochloride (DOX·HCl) was purchased from Zhejiang Hisun Pharmaceutical Co. Ltd. Hoechst 33258, amplex red reagent and 3-(4,5-dimethylthiazol-2-yl)-2,5-diphenylte-trazolium bromide (MTT) were purchased from Sigma-Aldrich Co. Reactive Oxygen Species Assay Kit was purchased from Beyotime. After being immersed with CaH_2 for 2 weeks, dichloromethane (DCM) and triethylamine (TEA) were dried by refluxing with CaH_2 and then distilled. Dimethylformamide (DMF) was dried by stirring with CaH_2 and then distilled under vacuum.

Measurement

^{1}H NMR spectra were recorded using a Bruker AVANCE DRX 400 spectrometer in $CDCl_3$, D_2O or DMSO-d_6 at 25 °C. Gel permeation chromatography (GPC) was measured in DMF using a series of liner Tskgel Super columns (AW3000 and AW5000) and Waters 515 HPLC pump with OPTILAB DSP Interferometric Refractometer (Wyatt Technology) as the detector. DMF containing 0.01 M LiBr was used as eluent with a flow rate of 1.0 mL min^{-1} at 50 °C. Transmission electron microscopy (TEM) images were performed on a JEOL JEM-1011 transmission electron microscope. Dynamic light scattering (DLS) measurements were tested on Brookhaven 90Plus size analyzer. UV-vis spectroscopy (UV-2450PC, Shimadzu) was used to measure the amount of DOX. Zeta potential measurements were conducted on a Malvern Zetasizer Nano ZS.

Synthesis of dialkyned-cystine derivative

2,2′-Dithiobis[1-(prop-2-ynylcarbamoyl)-ethyl-carbamicacid-*tert*-butyl ester] (monomer 1). The dialkyned-cystine derivative was synthesized according to a prior published literature with some modification.[31] A stirred solution of BOC-cystine (3.960 g, 9 mmol) and TEA (7 mL, 50.4 mmol) in 80 mL anhydrous DCM was chilled in an ice-bath, and propargylamine (2.5 mL, 36 mmol) was added portionwisely. Afterwards the mixture was kept at 0 °C upon addition of BOP reagent (9.558 g, 21.6 mmol) in 20 mL of DCM under argon for 0.5 h. The ice bath was removed after 2 h and the reaction was maintained at room temperature for 24 h. Dichloromethane was removed by reduced pressure distillation. The crude product was dissolved in 350 mL ethyl acetate, and the mixture was washed with saturated potassium hydrogensulphate ($KHSO_4$), saturated sodium dicarbonate ($NaHCO_3$) solution and saturated sodium chloride (NaCl). After drying over magnesium sulphate ($MgSO_4$), the solvent was removed by evaporation. Purification was achieved by column chromatography. Yield: 74.7%. ^{1}H NMR ($CDCl_3$, 400 MHz) δ1.48 (s, 18H), 2.18 (s, 2H), 2.94 (m, 4H), 4.08 (m, 4H), 4.92 (br s, 2H), 5.53 (d, 2H), 8.07 (br s, 2H).

Synthesis of bis(3-azidopropyl) oxalate (monomer 2)

Bis(3-azidopropyl) oxalate was synthesized according to the following steps. First, 3-chloro-1-propanol (9.454 g, 100 mmol), sodium azide (19.503 g, 300 mmol) and sodium hydroxide (1.000 g, 25 mmol) were added into 80 mL distilled water in a Schlenk flask. After stirring at 80 °C for 48 h, the product was extracted with diethyl ether. The combined organic extracts were washed with saturated sodium chloride (NaCl), and dried over $MgSO_4$. After volatiles evaporation, the colorless oil (3-azido-1-propanol) was obtained. Yield: 90%. ^{1}H NMR ($CDCl_3$, 400 MHz): δ(ppm) = 3.75 (t, 2H), 3.45 (t, 2H), 1.84 (m, 2H), 1.91 (s, 1H).

Second, bis(3-azidopropyl) oxalate was prepared according to the literature with minor modification.[32,33] A solution of oxalyl chloride (1.5 mL, 18 mmol) in 70 mL of DCM was added dropwisely to a well stirred ice-cold solution of 3-azido-1-propanol (3.030 g, 30 mmol), TEA (12.5 mL, 90 mmol) and DMAP (3.665 g, 3 mmol) in DCM (60 mL). The reaction was stirred vigorously at room temperature for 24 h under argon atmosphere. After filtration, the filtrate was washed with brine for five times and dried over $MgSO_4$. The obtained oil was purified by column chromatography. Yield: 73%. ^{1}H NMR ($CDCl_3$, 400 MHz): δ(ppm) = 4.4 (t, 2H), 3.46 (t, 2H), 2.02 (m, 2H).

Synthesis of azido-mPEG$_{2k}$ (mPEG$_{2k}$-N$_3$)

$mPEG_{2k}$-N_3 was synthesized as reported procedure with minor modification.[34] First, in a 250 mL dried Schlenk flask, TEA (13.9 mL, 100 mmol) was syringed into a solution of $mPEG_{2k}$ (10 g, 5 mmol) in 90 mL of DCM. Then the mixture was cooled to 0 °C in an ice bath before a DCM solution (90 mL) of mesyl chloride (3.9 mL, 50 mmol) was added dropwisely. After reaction at room temperature for 24 h, the solution was extracted with 20 mL of saturated brine for fourth. After drying the solution with $MgSO_4$, the concentrated solution was precipitated in diethyl ether and dried in vacuum for 24 h.

Second, the obtained methylsufonyl-$mPEG_{2k}$ (6.000 g, 3 mmol) and NaN_3 (9.751 g, 150 mmol) were dissolved in 30 mL dried DMF. The reaction mixture was degassed by three freeze–pump–thaw cycles and the reaction proceeded at 80 °C for 24 h.

After that, the reactive mixture was cooled to room temperature, and the excess amount of sodium azide and the side product (sodium bromide) were filtered off. After reduced pressure distillation, the mixture was dissolved in 300 mL of DCM, washed with saturated NaCl solution and dried over $MgSO_4$. The organic phase was concentrated, precipitated in 250 mL of diethyl ether and the product $mPEG_{2k}$-N_3 was dried in vacuum for 24 h. Yield: 71%. ^1H NMR ($CDCl_3$, 400 MHz): δ(ppm) = 3.64 (t, 181H), 3.38 (t, 4H).

Synthesis of polymer-RPDSP

Polycycloaddition reactions of the dialkyned monomer 1 with diazided monomer 2 were carried out under argon in Schlenk tube. In general, dialkyned monomer 1 (0.514 g, 1 mmol), diazided monomer 2 (0.256 g, 1 mmol), PMDETA (0.069 g, 0.4 mmol) and CuCl (0.020 g, 0.2 mmol) were reacted in 10 mL of dried DMF at 40 °C for 24 h after a deoxidation process. At the end of the polymerization, the degassed solution of dialkyned monomer 1 (0.103 g, 0.2 mmol) was added to the Schlenk tube to achieve dialkyne end groups on polymer. After precipitated in cold diethyl ether and filtered, the precipitation was washed with abundant water to obtain the product (hydrophobic block). In another Schlenk tube, the hydrophobic block (0.2 g) was reacted with $mPEG_{2k}$-N_3 (0.500 g, 0.25 mmol) under the catalysis of CuCl (0.050 g, 0.5 mmol), and PMDETA (0.173 g, 1 mmol) was used as chelating agents. The reaction was proceeded at 40 °C for 24 h. The products were purified by dialysis against DMF, ethylenediaminetetraacetic acid disodium salt (EDTA-2Na) (EDTA═Na) solution and pure water to remove the catalyst and unreacted $mPEG_{2k}$-N_3. After lyophilization, the final product (PRDSP) was obtained.

Determination of critical aggregation concentration (CAC) of PRDSP NPs

Critical aggregation concentration (CAC) of PRDSP NPs in deionized water was determined using pyrene as probe. PRDSP NPs were prepared with various concentrations (6.1×10^{-5} – 1.25×10^{-1} mg mL^{-1}) in deionized water, and the final concentration of pyrene was immobilized at 6.0×10^{-7} mol L^{-1}. The fluorescence spectra were monitored using a fluorescence spectrophotometer. The excitation spectra of PRDSP@pyrene solutions were scanned from 308 to 350 nm at room temperature. The intensity ratios of $I_{337.5}$ to I_{333} were plotted against the logarithm of PRDSP concentrations.

Preparation of the PRDSP and PRDSP@DOX NPs

Blank NPs were prepared by a modified nano-precipitation method. PRDSP (10 mg) was dissolved in 2 mL of DMF and stirred for 2 h. Deionized water (15 mL) was then added lentamente. The mixture was dialyzed against deionized water for 24 h at room temperature by using a dialysis membrane bag (MWCO 3500 Da).

DOX was loaded into PRDSP copolymer nanocarriers as a model drug by a dialysis method. Briefly, DOX·HCl (10 mg, 0.017 mmol) was stirred with TEA (7 μL, 0.051 mmol) in dimethyl sulfoxide (0.6 mL) for 2 h in the dark. The PRDSP copolymer (50 mg) was dissolved in DMF (2 mL). The mixture was stirred at room temperature overnight and then added dropwisely into 40 mL of deionized water. The solution was transferred into the dialysis bag (MWCO 3500) and dialyzed against deionized water for 24 h (the medium was changed every 3 h). The obtained DOX-loaded micelles (PRDSP@DOX NPs) were lyophilized in the dark.

Characterization of the PRDSP and PRDSP@DOX NPs

DLS was used to investigate size and size distribution of the NPs aggregates, and TEM was used to determine the morphological and size of the NPs aggregates. The TEM sample was prepared as follow: a drop of sample solution (0.5 mg mL^{-1}) was deposited onto a copper grid coated with carbon, and the sample was maintained at room temperature to volatilize the solvent.

PH and redox-triggered destabilization of PRDSP NPs

The size change of PRDSP NPs in response to pH, reduction agent (GSH), ROS (H_2O_2) was followed by DLS and TEM measurements.

For pH sensitivity, 20 mg of freeze dried NPs were dispersed in 40 mL of water solution (pH = 7.4 or 5.0). At predesigned time point, the change of PRDSP NP sizes was monitored by DLS. To determine the reduction-triggered destabilization of PRDSP NPs, 0, 10 μM, 100 μM or 10 mM GSH were appended to 5 mL solution of PRDSP NPs in Milli-Q (MQ). The solution was placed in a constant temperature shaker at 37 °C with a rotation speed of 100 rpm. To determine the oxidation sensitivity, PRDSPNPs were dispersed in MQ at specific concentrations (0.5 mg mL^{-1}), then certain amounts of H_2O_2 were added to make the final H_2O_2 concentrations to be 0, 0.1 and 10 mM, respectively. Eventually, to mimic blood and tumor circumstance, GSH were added to 5 mL of PRDSP NPs solutions in PBS (pH 7.4 or 5.0) to make the final GSH concentration to be 10 μM or 10 mM. The alteration of NP sizes was monitored in time by DLS, and the change of morphology under different conditions were observed using TEM.

The scavenging of H_2O_2

3 mg of PRDSP NPs or PRDSP@DOX NPs were suspended in 2 mL of H_2O_2 solutions (10 μM), and the solution was placed in a constant temperature shaker at 37 °C under gentle shaking. At appropriate time intervals, the solution was centrifuged (10 000 rpm) and the H_2O_2 concentration of the supernatant was determined by Amplex Red assay according to the manufacturer's protocol.

In vitro drug release

To determine the DLC and DLE, DOX-loaded polymer micelles were dissolved in DMF. The amount of DOX was quantified *via* fluorescence measurement according to a calibration curve. DLC and DLE of PRDSP NPs were calculated by the following equations:

$$\text{DLC (wt\%)} = (\text{weight of DOX in nanoparticles/total weight of DOX-loaded nannoparticles}) \times 100\%$$

$$\text{DLE (wt\%)} = (\text{weight of DOX in nanoparticles/total weight of DOX in feed}) \times 100\%$$

In vitro release profiles of DOX from PRDSP@DOX NPs were investigated in distinct buffer solutions (pH 7.4 phosphate buffer, pH 5.0 acetate buffer, pH 7.4 phosphate buffer with 10 μM of GSH, pH 7.4 phosphate buffer with 10 mM of GSH, pH 5.0 acetate buffer with 10 mM of GSH, MQ with 0, 100 μM or 10 mM of H_2O_2). The pre-weighed PRDSP@DOX NPs were suspended in 5 mL of corresponding buffer solution. The solution was subsequently transferred into a dialysis membrane bag (MWCO 3500 Da), and the dialysis bag was immersed into 50 mL of the homologous buffer solution. At predetermined time intervals, 2 mL of release medium was withdrawn for UV-vis analysis and then equal volume of fresh buffer was added. The concentration of released DOX was quantified using fluorescence measurement (λ_{ex} = 480 nm) base on the standard curve.

Cell lines

Three cell lines, L929 (mouse fibroblasts cells), A549 (non-small lung carcinoma cells) and HeLa (human cervical carcinoma cells) were selected for cell tests. L929, A549 and HeLa, which were offered by the Medical Department of Jilin University, China, were incubated in Dulbecco's modified Eagle's medium (DMEM, Gibco).

Reduction of cell ROS

The intracellular ROS production was measured by dichlorofluorescein-diacetate (DCFH-DA) staining. HeLa cells (5×10^5 cells per well) were seeded in a 6-well plates and incubated for 24 h. Cells were disposed with 20 μg or 200 μg of PRDSP NPs for 12 h and then treated with 5 μL of Rosup (1 mg mL^{-1}) for 10 h. Cells with only Rosup treatment were used as the positive control, and cells with no treatment were used as the negative control. 20 μM of DCFH-DA was added to each dish, and 1 h later, the fluorescence images were observed by confocal laser scanning microscope (CLSM). Flow cytometry was also performed to quantify the fluorescent cells.

Cell viability assays

In vitro cytotoxicity of PRDSP NPs against L929 and HeLa were assessed by methyltetrazolium (MTT) assay. Briefly, L929 cells were seeded onto 96-well microtiter plates at a density of 1×10^4 cells per well in 100 μL of DMEM and incubated at 37 °C and 5% CO_2 for 24 h. Then the culture medium was withdrawn. 100 μL of PRDSP solutions with different concentrations (0.0312–1 mg mL^{-1}) in complete DMEM were added. After being incubated for another 24 h in cell incubator, cells were subjected to MTT assay. The absorbance at 490 nm was measured (Bio-Rad 808 microplate reader) with control wells containing cell culture medium only. The relative cell viability was determined by comparing the absorbance at 490 nm. At the same time, cells were placed in 96-well plates (5×10^3 cells per well) in 100 μL of complete DMEM and incubated for 24 h to adhere, 100 μL of the PRDSP NPs at various concentrations were applied to replace the culture medium. After incubation for 48 h, MTT assay was used to evaluate cell viability.

The cytotoxicity of PRDSP@DOX NPs against HeLa and A549 cells were also determined by using a standard MTT assay. Briefly, four density (10×10^3, 7×10^3, 4×10^3, 2×10^3 cells per well) of HeLa cells were seeded in four 96-wells plates and incubated for 24 h. After the culture medium was discarded, cells were treated with 0 or 10 mM GSH for 2 h, and then rinsed with fresh DMEM. Free DOX and PRDSP@DOX at various concentrations were added. The MTT assay was carried out after incubation for 24, 48, 72 and 96 h, respectively. A549 cells were also used to evaluate the cytotoxicity of PRDSP@DOX NPs.

Intracellular drug release

CLSM and flow cytometric analyses were applied to monitor the cellular uptake and intracellular distribution of DOX and PRDSP@DOX NPs towards HeLa and A549 cells. For example, HeLa cells were seeded on the coverslips in 6-well plates (3×10^5 cells per well) and cultured in 2 mL of DMEM for 24 h, and then treated with GSH (10 mM) for 2 h. After washed by PBS, 2 mL of DOX or PRDSP@DOX NPs (at a final DOX concentration of 10 μg mL^{-1}) in DMEM were added, and cells were incubated for additional 0.5 or 4 h. Cells without GSH treatment were used as the control. In this study, the nuclei were stained by Hoechst 33258 (10 μg per well) and transferred to a blue color by software, accordingly, DOX was transferred to a red color. The images of cells were detected using a CLSM.

For flow cytometric analyses, the experimental process was similar to the preparation of CLSM samples with little modification. HeLa cells were placed into 6-well plates (3×10^5 cells per well) with no coverslip. After cultured for 24 h to adhere, preprocessed with 10 mM of GSH, and treated with 2 mL of DOX or PRDSP@DOX NPs (at a final DOX concentration of 10 μg mL^{-1}), cells were washed with PBS three times and trypsinized. Then, 1.0 mL of PBS was added, and the suspensions were centrifuged for 5 min at 1000 rpm and cells were re-suspended in 0.5 mL of PBS. The analysis was performed by flow cytometer. CLSM and flow cytometric analyses were also applied to investigate the cellular uptake and intracellular distribution of DOX and PRDSP@DOX NPs towards A549 cells.

Results and discussion

Preparation and characterization of "clickable" monomers and PRDSP triblock copolymer

In this work, dialkyned-cystine, diazide monomer and azide-terminated $mPEG_{2k}$ were applied to synthesis the linear redox dual-sensitive triblock copolymer PRDSP (Scheme 2) by CuAAC step polymerization with catalysis of CuCl.

Cystine was chosen as a raw material with amino groups protected by BOC to introduce the disulfide groups into polymer backbone. To avoid the racemization of L-cystine, BOP was selected as condensation agent instead of DCC or EDC. The

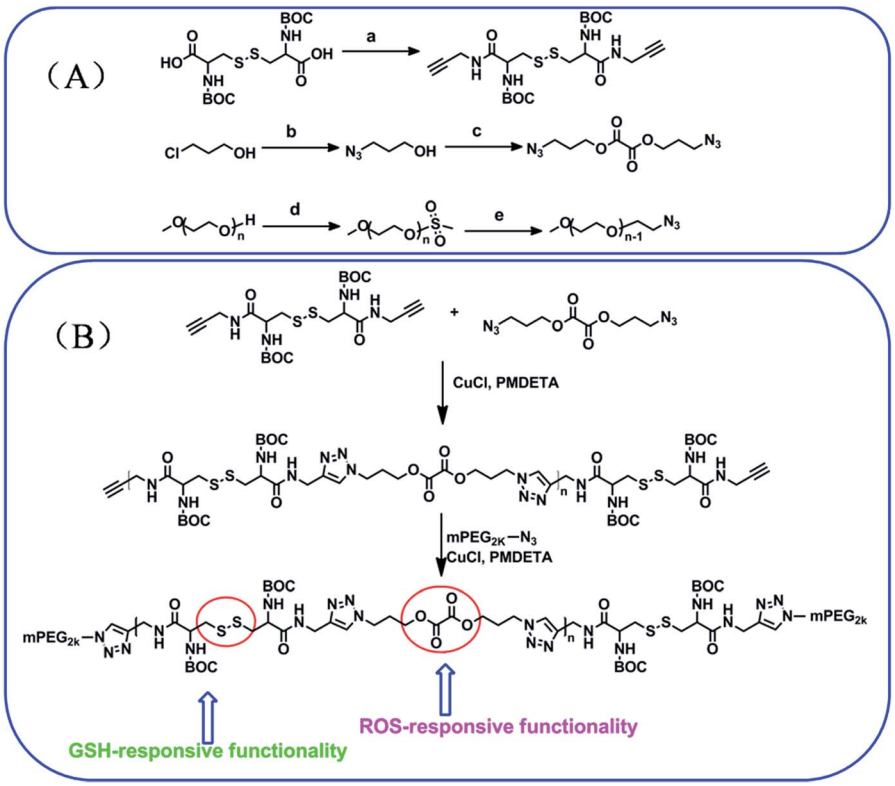

Scheme 2 Synthetic pathway for clickable monomers (A), ABA-type triblock copolymer PRSDP (B). Reagents and conditions: (a) proparygl amine, BOP, TEA, CH_2Cl_2, 0 °C for 2 h, room temperature (rt) for 24 h; (b) NaN_3, NaOH, H_2O, 80 °C for 48 h; (c) oxalylchloride, TEA, DMAP, CH_2Cl_2, 0 °C to rt for 24 h; (d) mesyl chloride, TEA, DMAP, CH_2Cl_2, 0 °C to rt for 24 h; (e) NaN_3, DMF, 80 °C for 24 h.

chemical structure of dialkyned-cystine was confirmed by ^{1}H NMR (Fig. S1A†). The signal corresponding to the alkynl group (2.18 ppm) could be clearly observed. The resonances at 4.08, 1.48 and 2.94 ppm were assigned to protons on CH_2 (–S–CH_2–), –BOC and CH_2 (–NH–CH_2) moiety, correspondingly. Fig. S1C† shows the ^{1}H NMR spectrum of the diazide monomer. All chemical shifts were assigned to the protons of diazide monomer, respectively. Fourier transform infrared spectroscopy (FT-IR) analysis of monomers was also performed (Fig. S2†). The appearance of azide peak at 2103 cm^{-1} further suggested the successful synthesis of azide-terminated monomers.

For CuAAC step polymerization, CuCl/PMDETA was used as the catalyst with minor excessive dialkyned monomer to produce alkyne groups on both ends of hydrophobic chain. Due to the hydrophobic property of the synthetic segment, abundant water was applied to wash the polymer to eliminate the catalyst. The acquired hydrophobic block was then reacted with azide-terminated $mPEG_{2k}$ to obtain the final amphiphilic triblock copolymer. For hydrophobic block, chemical shifts at 1.37 and 2.22 ppm in ^{1}H NMR were ascribed to the protons of BOC and CH_2 (adjacent to –CH_2–C═O), respectively (Fig. S3†). And the proton signals of the triazole ring at 8.0 and 8.44 ppm were explicitly observed. The ^{1}H NMR of PRDSP polymer also had the above chemical shifts with additional resonances at 3.52 ppm assigning to CH_2 (–CH_2–CH_2–O–) groups of $mPEG_{2k}$ (Fig. 1). The degree of polymerization (PD) was determined by calculating the relative peak area ratio of CH_2 ascribed to PEG to BOC groups (Fig. S3B†). PD was about 7.5, which corresponds to an average molecular weight of 9775 g mol^{-1}. The ^{1}H NMR spectra of PRDSP in D_2O was also measured (Fig. 1), and the resonances

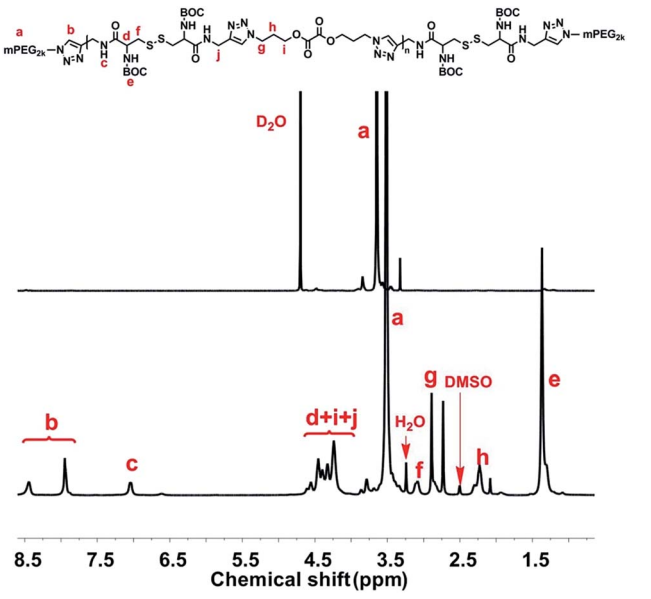

Fig. 1 ^{1}H NMR characterization of synthetic copolymer PRDSP in DMSO-d_6 and D_2O.

at 3.62 ppm were assigned to CH_2(–CH_2–CH_2–O–) groups of $mPEG_{2k}$. However, other signals on hydrophobic block were not clearly observed, implying the core–shell structure of PRDSP NPs in water. GPC was also used to investigate the number-average molecular weight (M_n) (Fig. S4†).

CAC measurement

To demonstrate the formation of micelles, pyrene was used as a hydrophobic fluorescence probe to investigate the critical aggregate concentration (CAC) value (Fig. S5†). CAC value of PRDSP was calculated to be 1.64 mg L^{-1}, which was obtained by plotting $I_{337.5}/I_{333}$ against the logarithm of PRDSP concentrations. The low CAC value illuminated good stability of the aggregates under highly diluted conditions, which was highly advantageous to intravenous administration.

Aggregates formation and characterization

Amphiphilic polymers are capable of self-assembly into aggregates in specific solvents. In this study, micelles of PRDSP block copolymers were prepared by the modified nanoprecipitation method. After completely dissolving the copolymer PRDSP in DMF, the deionized water was added lentamente. Then the mixture was dialyzed against the deionized water for 1 day to form the aggregate. DOX was used as a model anticancer drug for encapsulation. The aggregates' size, size distribution and the morphology were determined by DLS (Fig. 2A and S6A†) and TEM (Fig. 2B and S6B†). For blank PRDSP NPs, DLS measurements showed that PRDSP formed aggregates with size of 97 nm. In TEM micrographs, PRDSP NPs had clear spherical morphology with the average diameter around 70 nm. This phenomenon is ubiquitous and should ascribe to the shrinkage of the PEG shell during the sample preparation for TEM. After DOX encapsulation, the average size increased and the size distribution became broad. This phenomenon was common and also reported by other literatures.[35]

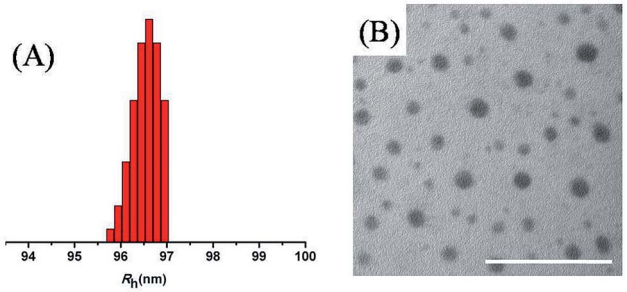

Fig. 2 (A) Average diameters of blank PRDSP NPs monitored by DLS, and (B) TEM micrograph of blank PRDSP NPs (scale bars: 500 nm).

Stability of PRDSP NPs

It has been confirmed that cancer tissue has idiosyncratic microenvironments including reduced extracellar and intracellar pH, increased temperature, elevated reductive agent level and oxidative stress. In this work, triazole, disulfide bond and oxalate structures were regularly and repeatedly positioned in polymer backbone, which could provide DDS with potential pH, reductive and oxidative sensitivities to release drugs around or inside tumor cells as much as possible. For this purpose, we investigated the triggered disassemble behavior of PRDSP NPs in response to different pH and concentration of GSH or H_2O_2.

The size change of PRDSP NPs in distinct condition as a function of time was followed by DLS measurement (Fig. 3). Infinitesimal variety was found for PRDSP NPs in the absence of GSH or in 10 μM of GSH. Particle size had enormous change while 100 μM GSH was added. Notably, when GSH was increased to 10 mM, fast aggregation was observed for PRDSP NPs. The size increased from 135 nm to 328 nm in 10 h, and reached to over 2900 nm after 14 h, showing significant reductive sensitivity (Fig. 3A). In the presence of 100 μM or 10 mM H_2O_2, PRDSP NPS also showed good oxidative responsiveness with immediately increased particle size (Fig. 3B). PRDSP NPs were quite stable with no size change at pH 7.4 with 10 μM of GSH to mimic the extracellular circumstance (Fig. 3C). When pH was decreased to 5.0, PRDSP NPs were found unstable with continuously increased particle size (Fig. 3C). The abundant triazole groups in polymer backbone would have stronger hydrogen-bond-accepting/-donating abilities compared with amide. These hydrogen bonds might be more sensitive and easier destroyed under lower pH, leading to instability of the NPs. In the case of treating with 10 mM of GSH at pH 5.0 to mimic the intracellular environment, significant size diversification (Fig. 3C) and broader size distribution (Fig. S7†) of PRDSP NPs were confirmed.

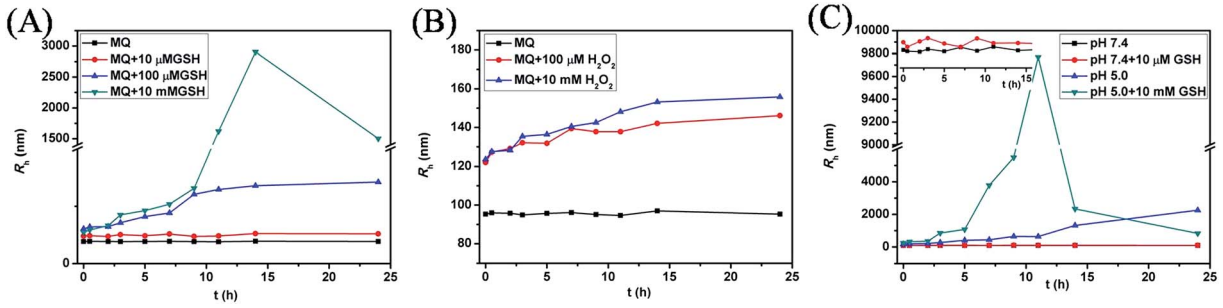

Fig. 3 Changes in average diameters of blank PRSDP NPs as a function of time (A) in MQ with different concentrations of GSH; (B) in MQ with different concentrations of H_2O_2; (C) in PBS at pH 7.4, pH 5.0 and conditions mimicking plasma and cancer cell environment monitored by DLS.

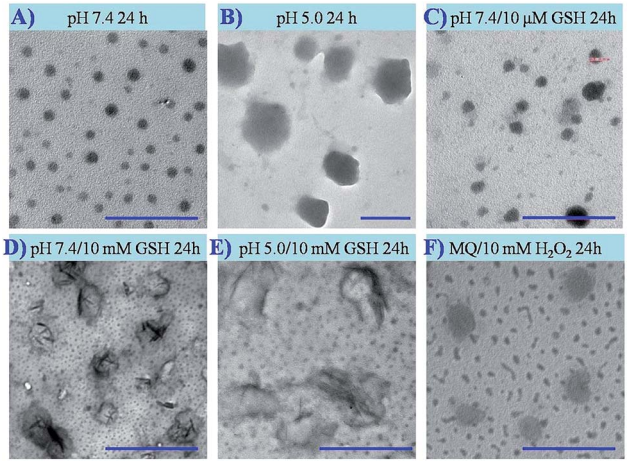

Fig. 4 The pH, GSH, ROS-sensitivity of PRDSP NPs monitored by TEM (scale bars: 500 nm).

It is assumed that when the disulfide bonds or oxalate structures in PRDSP backbone begun to be disrupted by the addition of GSH or H_2O_2, the stability of PRDSP NPs was destroyed, inducing the re-assembling or aggregation of NPs. While most disulfide bonds or oxalate structures in the main chain were consequently broken, the entire NPs structure could be dissociated, leading to smaller particle size. The diversification of the morphology and size of PRDSP NPs under different conditions was also monitored by TEM (Fig. 4). Similarly, PRDSP NPs were stable at pH 7.4 with little alteration in size, size distribution and morphology, but greatly changed with lowered pH and increased concentration of GSH or H_2O_2.

Another evidence for oxidative sensitivity of PRDSP NPs is H_2O_2 scavenging test by Amplex Red assay. Both blank PRDSP NPs and PRDSP@DOX could significantly reduce the concentration of H_2O_2 to 49 and 65% of its original level at 36 h, respectively (Fig. 5). H_2O_2 is one of the most important oxidative agents in cancer cell. It has been proved that peroxalate ester bond can be oxidized by H_2O_2 instantaneously and spontaneously, and eventually decomposed into CO_2.[36,37]

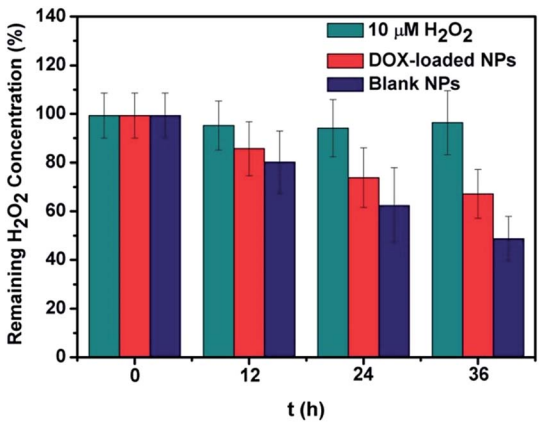

Fig. 5 H_2O_2 scavenging activity of PRDSP NPs.

The repeatedly located peroxalate ester bonds in PRDSP would therefore react with H_2O_2 to induce the cleavage of polymer backbone, and consequently reduce the H_2O_2-mediatedoxidative stress. All these results clearly demonstrated the redox dual-sensitive characteristics of the PRDSP NPs.

In vitro GSH, H_2O_2 triggered DOX release

DOX is one of the most potent and widely used anthracycline anticancer drugs to treat diverse types of solid malignant tumors by interacting with DNA or RNA to inhibit the macromolecular biosynthesis. In the current study, to confirm the feasibility of using the redox dual-sensitive PRDSP NPs for intracellular drug delivery, DOX was loaded into the PRDSP NPs as a model drug. DOX-loaded PRDSP NPs were prepared by dialysis method. The theoretical DOX loading content was set at 20 wt%. The results showed that DLC and DLE for PRDSP NPs were approximately 16% and 80%, respectively.

The pH, GSH, H_2O_2-dependent DOX release behaviors of the PRDSP@DOX were investigated by dialysis method under physiological condition (pH 7.4) and endosomal circumstance (pH 5.0) at 37 °C (Fig. 6). It has to be noted that it is difficult to introduce reductive and oxidative agents together in one system. Therefore, the drug release behaviors of PRDSP@DOX under reductive and oxidative stimulus have to be evaluated separately. A significant difference was observed for the DOX release profile at pH 7.4 and 5.0. This phenomenon could attribute to two factors. First, DOX had higher solubility in acidic media. Second, there are one primary amine, three carbonyl groups and five hydroxyl groups in one DOX molecule. These groups would have the possibility to form hydrogen bonds with triazole and amide groups on PRDSP, which are easier to be destroyed under acidic condition. About 49% of DOX was released from PRDSP@DOX NPs at pH 5.0 in 75 h. While in the case of pH 7.4, the released DOX was only 15%.

PH 7.4 and 10 μM GSH were used again to mimic the physiological condition. Less than 15% of DOX was released in 75 h, suggesting the satisfying stability of PRDSP@DOX during blood circulation. Increasing of GSH concentration (10 mM, pH 7.4) would definitely accelerate the release speed. In the presence of 10 mM of GSH at pH 5.0 to mimic the intracellular environment, DOX release had the fastest speed. More than 82% of DOX was released in 75 h, indicating the excellent reductive sensitivity of PRDSP@DOX NPs triggered by GSH. H_2O_2-triggered DOX release from PRDSP@DOX NPs was monitored in the absence or presence of H_2O_2 in MQ (Fig. 6B). The results showed that PRDSP@DOX released DOX more rapidly in H_2O_2. In 75 h, about 44% and 20% of DOX were released in the presence of 10 mM and 100 μM of H_2O_2. The above results indicated that drug release from PRDSP@DOX could be controlled under the acidic and redox conditions. The well displayed multi-sensitivities endow this system with excellent characteristics for smart intracellular drug delivery in tumor cells.

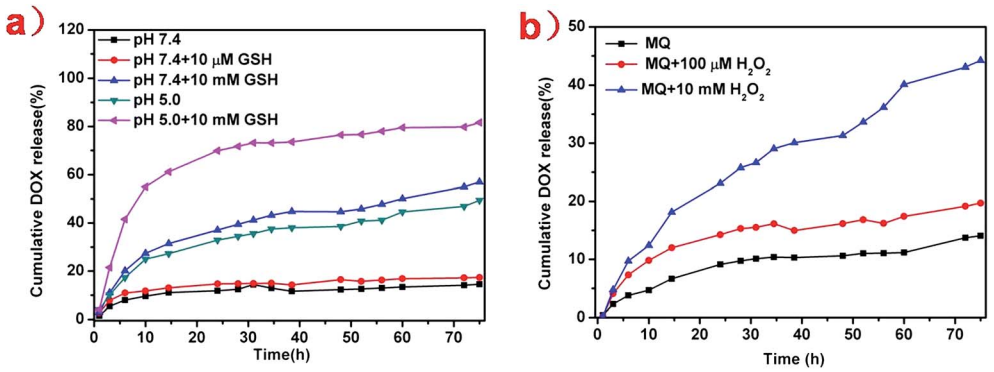

Fig. 6 *In vitro* DOX release under different conditions.

Inhibition of intracellular ROS

The impactful treatment of inflammation and other ROS-related diseases, such as malignant tumor, requires effective suppression or elimination of ROS production. In order to estimate the potential of PRDSP NPs as ROS scavenger, we investigated their ability to suppress ROS generation in HeLa cells stimulated by Rosup as an endotoxin. DCFH-DA was used as ROS probe to test the level of ROS generated in cells. DCFH-DA is non-fluorescent until it can be oxidized by the intracellular ROS. The production of ROS in cells was determined by CLSM and flow cytometry. After Rosup treatment for 12 h, a tremendous amount of ROS was produced in cells, which was evidenced by the stronger DCFH fluorescence in CLSM images (Fig. 7). 20 μg of PRDSP NPs showed slightly inhibitory effects on ROS generation. However, when 200 μg of PRDSP NPs was added, the remarkably reduced red fluorescence in cells was observed, suggesting the reliable potent of PRDSP as ROS scavenger. Flow cytometry results (Fig. S8†) were consistent with CLSM results.

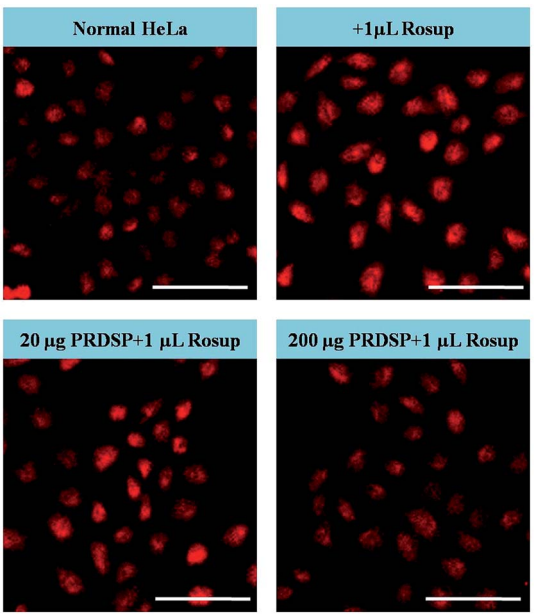

Fig. 7 Reduction of intracellular ROS, representative CLSM images of Rosup-stimulated cells stained with DCFH-DA (bar: 100 μm).

In vitro cellular proliferation assay

The cytotoxicity of the blank PRDSPNPs was evaluated using L929 cells and HeLa cells (Fig. 8). The viabilities of L929 and HeLa cells treated with PRDSP NPs for 24 h and 48 h exceeded 80% at all test concentrations up to 1 mg mL^{-1}, showing negligible cytotoxicity and favourable compatibility and safety of PRDSP NPs to cells (Table 1).

In vitro cellular proliferation inhibitions of free DOX, PRDSP@DOX against HeLa and A549 cells (Fig. 9 and S10†) were also evaluated. To confirm the intracellular concentration of GSH uniformly, cells were first pretreated with 10 mM of GSH for 2 h and then incubated with free DOX or PRDP@DOX NPs (gradient concentrations from 10 to 0.156 μg mL^{-1}) for predetermined time. Cells with no pretreatment were used as control. In all groups, higher drug dose would lead to increased cytotoxicity. Unlike the free diffusion of free DOX into cell, DOX released from PRDSP@DOX is a time consuming procedure. PRDSP@DOX thus exhibited slightly lower cell inhibition efficiency than free DOX. The IC_{50} values (half maximal (50%) inhibitory concentration) of different samples with different cultural time were listed in Table 2. The results showed that compared with non-pretreated groups, PRDSP@DOX NPs in the presence of GSH exhibited higher

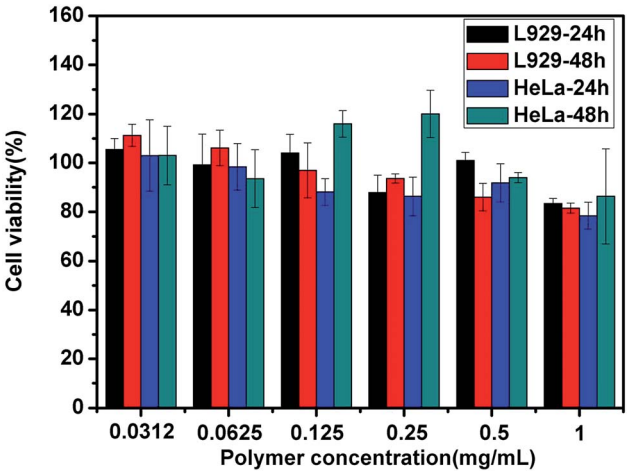

Fig. 8 *In vitro* cytotoxicities of PRDSP NPs to L929 and HeLa cells.

Table 1 Information about the synthetic copolymer and DOX-loaded NPs

Entry	Copolymer	M_n[a] (g mol^{-1}) ^{1}H NMR	M_n[b] (g mol^{-1}) GPC	CAC[c] (10^{-3} mg mL^{-1})	Diameters[d] (nm)	DLC[e] (wt%)	DLE (wt%)
1	PRDSP	9775	22 750	1.64	97	16	80

[a] Calculated by ^{1}H NMR with DMSO-d_6 as the solvent. [b] Calculated by GPC with DMF as the eluent. [c] Detected by luminescence spectrometer using pyrene as probe. [d] Determined by DLS. [e] Determined by UV-vis spectroscopy with assistance of calibration curve.

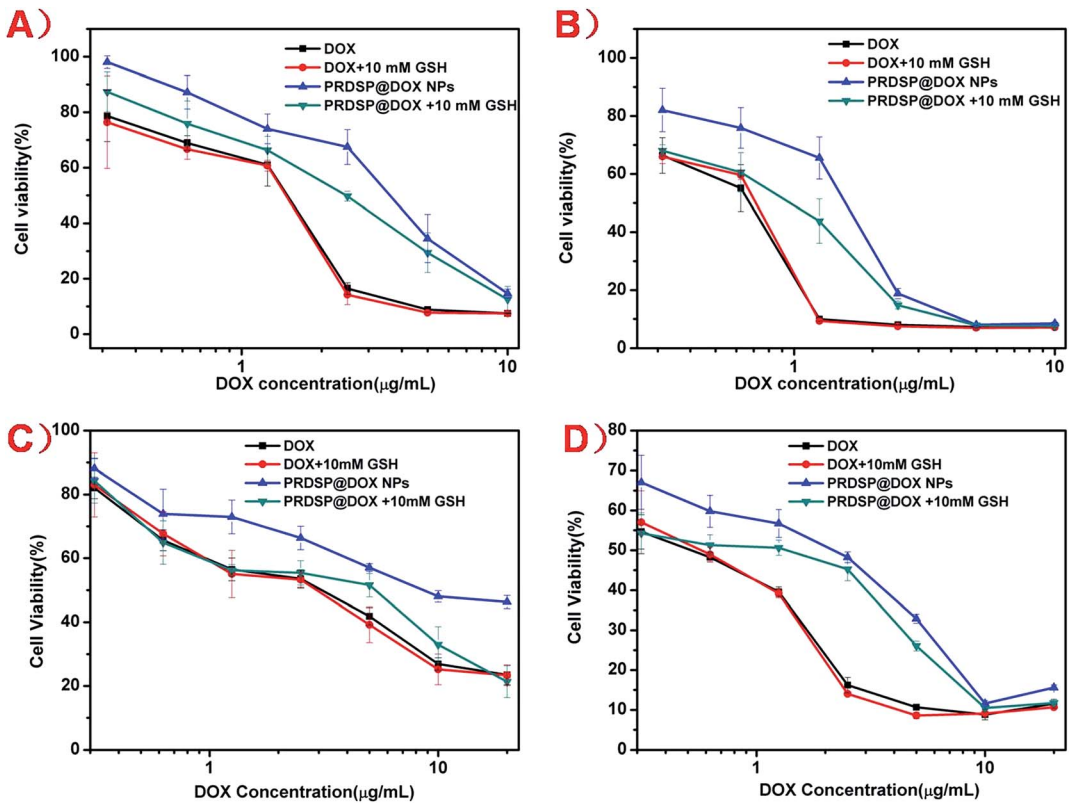

Fig. 9 *In vitro* cytotoxicity of PRDSP@DOX NPs and free DOX·HCl at various DOX concentrations towards 10 mM GSH-pretreated or non-pretreated cells with different incubation time. (A) HeLa, 24 h; (B) HeLa, 48 h; (C) A549, 24 h; (D) A549, 48 h.

inhibition efficacy with significantly decreased IC_{50} values. While in control groups, the pretreatment of GSH had no impact on the cytotoxicity of HeLa/A549 cells cultured with free DOX. The results demonstrated that faster DOX release from PRDSP@DOXNPs could be well triggered by the higher intracellular reduction agent level.

Intracellular DOX release

To determine whether PRDSP NPs were effective to deliver DOX into cells, the cellular internalization of DOX and PRDSP@DOX NPs towards HeLa cells were monitored by CLSM and flow cytometry. HeLa cells were incubated with DOX or PRDSP@DOX in the absence or presence 10 mM of GSH for

Table 2 IC_{50} values of DOX and PRDSP@DOX NPs towards 10 mM GSH pretreated or non-pretreated HeLa/A549 cells for different incubation time

	HeLa cells		A549 cells	
	IC_{50} (μg mL^{-1}) 24 h	IC_{50} (μg mL^{-1}) 48 h	IC_{50} (μg mL^{-1}) 24 h	IC_{50} (μg mL^{-1}) 48 h
DOX	1.44	0.68	3.08	0.50
DOX + 10 mM GSH	1.48	0.75	3.17	0.58
PRDSP@DOX NPs	3.58	1.67	8.92	2.17
PRDSP@DOX + 10 mM GSH	2.41	1.02	5.32	1.34

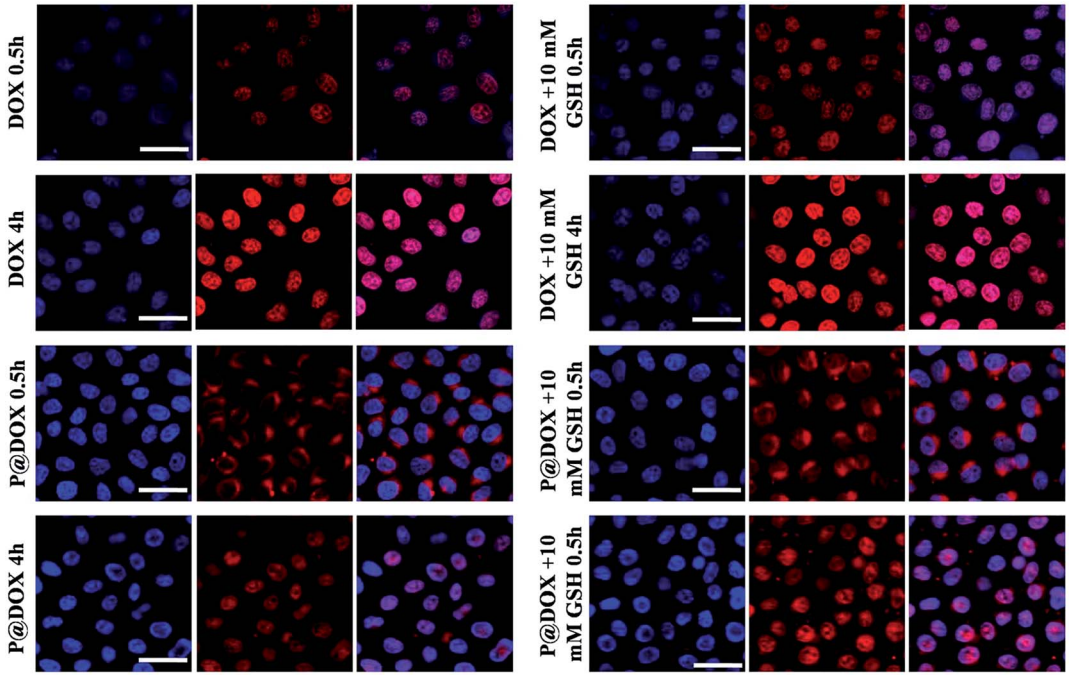

Fig. 10 Cellular uptake of DOX and PRDSP@DOX NPs in the presence or absence of 10 mM GSH towards HeLa cells (blue: Hoechst, red: DOX. Bar: 50 μm).

the designed time, and detected using CLSM (Fig. 10). As expected, stronger red fluorescence in cells was clearly observed with increased incubation time. After 0.5 or 4 h incubation with free DOX, the DOX fluorescence was observed to be aggregated in the nuclei in both samples. There was no difference between non-pretreated and GSH pretreated groups. In the case of PRDSP@DOX groups, stronger intracellular DOX fluorescence in GSH pretreated cells was observed, in comparison with non-pretreated group. After incubation with PRDSP@DOX for 0.5 h, DOX fluorescence was found to be aggregated basically around the nuclei. With increasing culture time to 4 h, DOX fluorescence mostly emerged in the nuclei. These data suggested that PRDSP NPs was potent to deliver DOX into cells. For further confirmation, cellular uptake of DOX and PRDSP@DOX NPs into HeLa cells were determined by flow cytometry (Fig. S9†), and accordant results were acquired. As shown in Fig. S9,† for free DOX, there was no fluorescence intensity distinction between non-pretreated and 10 mM GSH pretreated group. And for PRDSP@DOX NPs, the fluorescence intensity decreased in the following order: PRDSP@DOX in 10 mM GSH pretreated cells (cultured for 4 h) > PRDSP@DOX in GSH non-pretreated cells (cultured for 4 h) > PRDSP@DOX in 10 mM GSH pretreated cells (cultured for 0.5 h) > PRDSP@DOX in GSH non-pretreated cells (cultured for 0.5 h). Several researchers have reported that, compared with the DOX in NPs at the same concentration, the free DOX have stronger fluorescence due to the self-quenching effect of DOX.[38] The intracellular DOX release from PRDSP@DOX towards A549 cells was also investigated by CLSM (Fig. S11†). The results also showed that the PRDSP@DOX NPs could be internalized by A549 cells. All the results indicated that the synthetic copolymer PRDSP was a biologically responsive anticancer drug carrier and could realize controlled drug release.

Conclusion

A novel biologically responsive triblock copolymer PRDSP was fabricated as a biocompatible and biodegradable drug delivery carrier. The amphiphilic copolymer PRDSP was synthesized *via* CuAAC click polymerization, and disulfide bond, peroxalate ester and triazole units were repeatedly positioned in the main-chain of hydrophobic blocks. DLS, TEM, GPC results clearly showed responsiveness of PRDSPNPs under acidic or redox conditions. DOX was loaded into the PRDSP NPs as a model drug, and could be responsively released in the presence of biologically relevant concentrations of GSH and H_2O_2. Lower pH would also accelerate the DOX release speed. *In vitro* cellular experiment confirmed that PRDSP NPs was ROS-sensitive. MTT, CLSM and flow cytometry results indicated that the internalization and the anticancer efficacy of PRDSP@DOX NPs were enhanced in the presence of 10 mM GSH. The investigation indicated that the PRDSP NPs were potent drug delivery systems with heterogeneity-sensitivity for cancer therapy.

Acknowledgements

The authors would like to thank the financial support from National Natural Science Foundation of China (no. 51321062 and 21174143), the Ministry of Science and Technology of China (863 Project, no. SS2012AA020603), and "100 Talents

Program" of the Chinese Academy of Sciences (no. KGCX2-YW-802).

Notes and references

1 K. Chen, J. Xu, J. C. Luft, S. Tian, J. S. Raval and J. M. DeSimone, *J. Am. Chem. Soc.*, 2014, **136**, 9947–9952.
2 L. Cui, J. A. Cohen, K. E. Broaders, T. T. Beaudette and J. M. J. Fréchet, *Bioconjugate Chem.*, 2011, **22**, 949–957.
3 K. Dan and S. Ghosh, *Angew. Chem., Int. Ed.*, 2013, **52**, 7300–7305.
4 S. J. Lee, K. H. Min, H. J. Lee, A. N. Koo, H. P. Rim, B. J. Jeon, S. Y. Jeong, J. S. Heo and S. C. Lee, *Biomacromolecules*, 2011, **12**, 1224–1233.
5 K. Lu, M. Cao, W. Mao, X. Sun, J. Tang, Y. Shen and M. Sui, *J. Mater. Chem.*, 2012, **22**, 15804–15811.
6 Z. Lin, W. Gao, H. Hu, K. Ma, B. He, W. Dai, X. Wang, J. Wang, X. Zhang and Q. Zhang, *J. Controlled Release*, 2014, **174**, 161–170.
7 H. Xiao, G. T. Noble, J. F. Stefanick, R. Qi, T. Kiziltepe, X. Jing and B. Bilgicer, *J. Controlled Release*, 2014, **173**, 11–17.
8 W. Hong, D. Chen, L. Jia, J. Gu, H. Hu, X. Zhao and M. Qiao, *Acta Biomater.*, 2014, **10**, 1259–1271.
9 H. S. Han, T. Thambi, K. Y. Choi, S. Son, H. Ko, M. C. Lee, D.-G. Jo, Y. S. Chae, Y. M. Kang, J. Y. Lee and J. H. Park, *Biomacromolecules*, 2015, **16**, 447–456.
10 P. Liu, B. Shi, C. Yue, G. Gao, P. Li, H. Yi, M. Li, B. Wang, Y. Ma and L. Cai, *Polym. Chem.*, 2013, **4**, 5793–5799.
11 G. Liu, X. Wang, J. Hu, G. Zhang and S. Liu, *J. Am. Chem. Soc.*, 2014, **136**, 7492–7497.
12 D. Ling, W. Park, S.-j. Park, Y. Lu, K. S. Kim, M. J. Hackett, B. H. Kim, H. Yim, Y. S. Jeon, K. Na and T. Hyeon, *J. Am. Chem. Soc.*, 2014, **136**, 5647–5655.
13 M. Li, Z. Tang, S. Lv, W. Song, H. Hong, X. Jing, Y. Zhang and X. Chen, *Biomaterials*, 2014, **35**, 3851–3864.
14 S. Lv, Z. Tang, D. Zhang, W. Song, M. Li, J. Lin, H. Liu and X. Chen, *J. Controlled Release*, 2014, **194**, 220–227.
15 W. Chen, P. Zhong, F. Meng, R. Cheng, C. Deng, J. Feijen and Z. Zhong, *J. Controlled Release*, 2013, **169**, 171–179.
16 R. Cheng, F. Meng, C. Deng, H.-A. Klok and Z. Zhong, *Biomaterials*, 2013, **34**, 3647–3657.
17 F. Meng, W. E. Hennink and Z. Zhong, *Biomaterials*, 2009, **30**, 2180–2198.
18 J. Fang, T. Seki and H. Maeda, *Adv. Drug Delivery Rev.*, 2009, **61**, 290–302.
19 C. de Gracia Lux, S. Joshi-Barr, T. Nguyen, E. Mahmoud, E. Schopf, N. Fomina and A. Almutairi, *J. Am. Chem. Soc.*, 2012, **134**, 15758–15764.
20 E. Ko, D. Jeong, J. Kim, S. Park, G. Khang and D. Lee, *Biomaterials*, 2014, **35**, 3895–3902.
21 J. Kwon, J. Kim, S. Park, G. Khang, P. M. Kang and D. Lee, *Biomacromolecules*, 2013, **14**, 1618–1626.
22 N. Ma, Y. Li, H. Ren, H. Xu, Z. Li and X. Zhang, *Polym. Chem.*, 2010, **1**, 1609–1614.
23 H.-K. Yang and L.-M. Zhang, *Mater. Sci. Eng., C*, 2014, **41**, 36–41.
24 G. H. Gao, M. J. Park, Y. Li, G. H. Im, J.-H. Kim, H. N. Kim, J. W. Lee, P. Jeon, O. Y. Bang, J. H. Lee and D. S. Lee, *Biomaterials*, 2012, **33**, 9157–9164.
25 J. Wang, X. Sun, W. Mao, W. Sun, J. Tang, M. Sui, Y. Shen and Z. Gu, *Adv. Mater.*, 2013, **25**, 3670–3676.
26 V. V. Rostovtsev, L. G. Green, V. V. Fokin and K. B. Sharpless, *Angew. Chem., Int. Ed.*, 2002, **41**, 2596–2599.
27 X.-M. Liu, L.-d. Quan, J. Tian, F. C. Laquer, P. Ciborowski and D. Wang, *Biomacromolecules*, 2010, **11**, 2621–2628.
28 C. Deraedt, A. Rapakousiou, Y. Wang, L. Salmon, M. Bousquet and D. Astruc, *Angew. Chem.*, 2014, **53**, 8445–8449.
29 H.-k. Li, J.-z. Sun, A.-j. Qin and B. Tang, *Chin. J. Polym. Sci.*, 2012, **30**, 1–15.
30 Y. Wang, R. Zhang, N. Xu, F.-S. Du, Y.-L. Wang, Y.-X. Tan, S.-P. Ji, D.-H. Liang and Z.-C. Li, *Biomacromolecules*, 2010, **12**, 66–74.
31 Y. Wu, H. Kuang, Z. Xie, X. Chen, X. Jing and Y. Huang, *Polym. Chem.*, 2014, **5**, 4488–4498.
32 R. Martín, L. B. Jiménez, M. Álvaro, J. C. Scaiano and H. García, *Chem.–Eur. J.*, 2009, **15**, 8751–8759.
33 E. Brenna, C. Fuganti, F. G. Gatti and F. Parmeggiani, *Tetrahedron: Asymmetry*, 2009, **20**, 2694–2698.
34 Z. Zhang, X. Chen, L. Chen, S. Yu, Y. Cao, C. He and X. Chen, *ACS Appl. Mater. Interfaces*, 2013, **5**, 10760–10766.
35 B. Li, Q. Wang, X. Wang, C. Wang and X. Jiang, *Carbohydr. Polym.*, 2013, **93**, 430–437.
36 P. v. Czarnecki, A. Kampert, S. Barbe and J. C. Tiller, *Tetrahedron Lett.*, 2011, **52**, 3551–3554.
37 Y. B. Tsaplev, *J. Anal. Chem.*, 2012, **67**, 506–514.
38 J. Ding, F. Shi, C. Xiao, L. Lin, L. Chen, C. He, X. Zhuang and X. Chen, *Polym. Chem.*, 2011, **2**, 2857–2864.